

# Atomic Force Microscopy Studies of Hydration of Fluorinated Amide/Urethane Copolymer Film Surfaces

Boris B. Akhremitchev, Brian K. Mohney, Kacey G. Marra,  
Toby M. Chapman, and Gilbert C. Walker\*

Department of Chemistry, University of Pittsburgh, Pittsburgh, Pennsylvania 15260

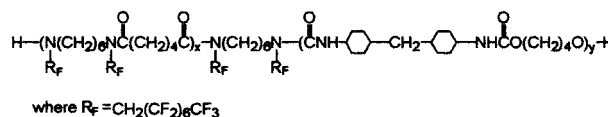
Received August 12, 1997. In Final Form: June 9, 1998

A poly(amide urethane) block copolymer has been studied using atomic force microscopy and infrared spectroscopy to examine the effects on the surface of immersion underwater. A film initially prepared in air and annealed above the glass transition temperature undergoes significant surface morphology change upon immersion, with noteworthy formation of surface particles. The particles are compliant and reduce surface friction probed by atomic force microscopy. The pH dependence of the force of adhesion of the atomic force microscope tip to the polymer is examined and found to vary with surface morphology and with tip functionality. Double layer forces as well as tip-induced extensions of the polymeric particle are identified. The infrared measurements indicate that both hydrophobic and hydrophilic blocks are partially hydrated within minutes and undergo further hydration on longer time scales, up to days.

## Introduction

Surface rearrangement of a poly(amide urethane) block copolymer film caused by submersion under water has been characterized by atomic force microscopy (AFM) and infrared spectroscopy (IRS). AFM using chemically modified tips<sup>1–12</sup> reveals changes in the surface adhesion properties and particle formation. IRS reveals water penetration into the polymer film via hydrogen/deuterium exchange effects on polymer functional group IR absorbances. The combination of AFM and IRS promises to provide insight into previously observed<sup>13–15</sup> contact angle hysteresis. The block copolymers under study have been designed with dual goals: to have low free energies of exposed surfaces and also to adhere to substrates.<sup>14</sup> Meeting these two goals in a single-coating material is important in many applications where biofouling is troublesome, including marine and implant environments. Understanding the forces between hydrophobic and hy-

Chart 1. Poly(amide urethane) Block Copolymer<sup>13</sup>



drophilic region of copolymers, and the role hydration plays in their dynamics, is of fundamental importance.<sup>16</sup> Recent efforts<sup>17–21</sup> have highlighted the roles of adsorbed species on surface free energies.

Specifically, we report on the poly(amide urethane) copolymer with fluorinated side chains shown in Chart 1. The urethane is referred to as the “hard” block and the nylon is the “soft” block.

Electron spectroscopy for chemical analysis (ESCA) studies on cast, annealed films of these copolymers by Gardella and co-workers have shown segregation of the fluorinated polyamide soft segment to the air-exposed surface.<sup>13</sup> Low critical surface tensions have been determined by goniometric contact angle measurements that employ a series of alkanes.<sup>14</sup> Studies on these and related copolymer films using the Wilhelmy technique have shown high water advancing contact angles.<sup>14</sup>

One of the intriguing properties that these copolymers exhibit is contact angle *hysteresis*.<sup>14,16,22</sup> That is, the history of exposure of the surface to water affects the observed water contact angle. This hysteresis can have thermodynamic or kinetic origins. Thermodynamic hysteresis is caused by surface heterogeneity and roughness. Kinetic hysteresis is usually explained by assuming that immersing the copolymer in water causes modification of surface properties such as from penetration of water into

\* To whom correspondence should be addressed. Supported by the Office of Naval Research, Grants N0001-96-1-0735 and N00014-92-J-1316.

(1) Vezenov, D. V.; Noy, A.; Rozsnyai, L. F.; Lieber, C. M. *J. Am. Chem. Soc.* **1997**, *119*, 2006–2015.

(2) Frisbie, C. D.; Rozsnyai, L. F.; Noy, A.; Wrighton, M. S.; Lieber, C. M. *Science* **1994**, *265*, 2071.

(3) Noy, A.; Frisbie, C. D.; Rozsnyai, L. F.; Wrighton, M. S.; Lieber, C. M. *J. Am. Chem. Soc.* **1995**, *117*, 7943.

(4) Vezenov, D. V.; Noy, A.; Rozsnyai, L. F.; Lieber, C. M. *J. Am. Chem. Soc.* **1997**, *119*, 2006.

(5) Green, J.-B.; McDermott, M. T.; Porter, M. D. *J. Phys. Chem.* **1996**, *100*, 13342.

(6) Siqueira, D. F.; Kohler, K.; Stamm, M. *Langmuir* **1995**, *11*, 3092.

(7) Green, J.-B.; McDermott, M. T.; Porter, M. D.; Siperko, L. M. *J. Phys. Chem.* **1995**, *99*, 10960.

(8) Han, T.; Williams, J. M.; Beebe, T. P., Jr. *Anal. Chim., Acta* **1995**, *307*, 365.

(9) Thomas, R. C.; Houston, J. E.; Crooks, R. M.; Kim, T.; Michalske, T. A. *J. Am. Chem. Soc.* **1995**, *117*, 3830.

(10) Akari, S.; Horn, D.; Keller, H.; Schrepp, W. *Adv. Mater.* **1995**, *7*, 549.

(11) Sinniah, S. K.; Steel, A. B.; Miller, C. J.; Teutt-Robey, J. E. *J. Am. Chem. Soc.* **1996**, *118*, 8925.

(12) van der Vegte, E. W.; Hadziioannou, G. *J. Phys. Chem. B* **1997**, *101*, 9563.

(13) Zhuang, H.; Marra, K. G.; Ho, T.; Chapman, T. M.; Gardella, J. A., Jr. *Macromolecules* **1996**, *29*, 1660.

(14) Chapman, T. M.; Marra, K. G. *Macromolecules* **1995**, *28*, 2081–2085.

(15) Chapman, T. M.; Bernrashed, R.; Marra, K. G.; Keener, J. P. *Macromolecules* **1995**, *28*, 331–335.

(16) Israelachvili, J. *Intermolecular and Surface Forces*; Academic Press: New York, 1992.

(17) Cao, T.; Yin, W.; Armstrong, J. L.; Webber, S. E. *Langmuir* **1994**, *10*, 1841.

(18) Iyengar, D. R.; Perutz, S. M.; Dai, C. A.; Ober, C. K.; Kramer, E. J. *Macromolecules* **1996**, *29*, 1229.

(19) Siqueira, D. F.; Koehler, K.; Stamm, M. *Langmuir* **1995**, *11*, 3092.

(20) Sharma, B. G.; Basu, S.; Sharma, M. M. *Langmuir* **1996**, *12*, 6506.

(21) Park, D.; Keszler, B.; Galiatsatos, V.; Kennedy, J. P.; Ratner, B. D. *Macromolecules* **1995**, *28*, 2595. Ratner B. D. *Ann. Biomed. Eng.* **1983**, *11*, 313.

(22) Tretinnikov, O. N.; Ikada, Y. *Langmuir* **1994**, *10*, 1606.

a surface layer or reorientation of surface functional groups. The water contact angle hysteresis for the polymer in Chart 1 was shown to be ca. 30° by goniometry and ca. 60° by the Wilhelmy<sup>14</sup> method. A significant fraction of water droplet spreading on this copolymer occurred within seconds.<sup>14</sup>

### Experimental Section

**Sample Preparation.** The poly(amide urethane) shown in Chart 1 was spin-cast into films from 10% (w/v) solutions in 1,1,1,3,3,3-hexafluoro-2-propanol using a Headway Research, Inc., ED101D photoresist spinner at a spin rate of 4000 rpm and annealed in an Abderhalden pistol for a minimum of 48 h at several degrees above  $T_g$ , 182.8 °C. The film substrates were mica or iron for the AFM measurements and calcium fluoride for the IR measurements. All water was deionized with a Barnstead NANOpure filtration unit to 18 MΩ cm resistivity. Constant ionic strength buffer solutions were prepared from sodium acetate, acetic acid, and water. Hydration experiments were performed by continuous immersion under aqueous solution.

**Atomic/Chemical Force Microscopy.** Height, adhesion, and friction measurements were performed with a Digital Instruments (Santa Barbara, CA) Nanoscope IIIa Multimode scanning force microscope equipped with a fluid cell. Methyl and carboxylic acid coated probe tips were purchased from BioForce Laboratory. Images of the tip were obtained on the silicon tip grating (grating tip radius is specified <10 nm by the manufacturer, NT-MDT Co.) and inspected to extract the cantilever tip radius. Tip radius was determined to be ca. 50 nm. We do not presume or require knowledge of the tip radius in our analysis. The normal spring constants of the triangular, 120 and 200 μm long Si<sub>3</sub>N<sub>4</sub> cantilevers, ca. 0.05 and 0.13 N/m, respectively, were obtained by the resonant frequency detection method.<sup>23</sup>

**AFM Data Analysis.** Software provided with the Nanoscope IIIa microscope was used to collect height, lateral force, and force vs distance curves (often called force plots). For each experiment we collected 4096 force vs distance curves as a function of the tip position on the surface. The data are subsequently analyzed using custom software.

Force curves were collected for scanner approach and retract. From tip-sample separation force plots we calculate the adhesion energy and dissipated energy using JKR theory<sup>24</sup> (after the work of Jonson, Kendal, and Roberts, 1971). We assume here that the polymer film is elastic and that the tip shape can be approximated as a sphere. We do not make assumptions about the tip radius of curvature.

According to JKR theory a spherical tip under load  $F$  on the surface indents an elastic surface with a contact area radius  $a$  given by<sup>24</sup>

$$a^3 = \frac{R}{K} [F + 3\pi R W_{12} + \sqrt{6\pi R W_{12} F + (3\pi R W_{12})^2}] \quad (1)$$

where  $K$  is the elastic modulus of the surface,  $R$  is the tip radius of curvature, and  $W_{12}$  is the adhesion work per unit area. The tensile load applied when the tip-sample contact breaks—adhesion force—can be estimated as the minimum real solution to eq 1.<sup>24</sup> Therefore the adhesion work per unit area can be calculated:

$$W_{12} = -\frac{2F_{adh}}{3\pi R} \quad (2)$$

Substituting (2) into (1) the adhesion contact area radius is

$$a_{adh} = \sqrt[3]{\frac{R}{K} [-F_{adh}]} \quad (3)$$

The indentation of the sample,  $\delta$ , is given by<sup>25</sup>

$$\delta = \frac{a^2}{3R} + \frac{2F}{3aK} \quad (4)$$

From this expression the spring constant of the tip-sample interaction  $k_i$ <sup>26</sup> can be obtained

$$1/k_i = d\delta/dF \quad (5)$$

This spring constant can be calculated in the case of zero applied load,  $F = 0$ , using (5), (4), and (1), which includes an elastic component together with a component due to contact area change. This gives an expression for contact area radius at zero applied load

$$a_{F=0} = \frac{10}{9} \frac{k_{i,F=0}}{K} \quad (6)$$

The ratio of the contact area radius at zero applied force to the radius when the tip-sample contact breaks is<sup>24</sup>

$$a_{F=0}/a_{adh} = \sqrt[3]{4} \quad (7)$$

The total energy of adhesion,  $W = W_{12}\pi a_{adh}^2$ , using eqs 2, 1, 7, and 6, is

$$W = \sqrt[3]{4} \frac{6}{10} \frac{F_{adh}^2}{k_{i,F=0}} \quad (8)$$

which is independent of the tip radius  $R$  and the radius of the tip-sample interaction area  $a$  and depends only upon measurable quantities: adhesion force  $F_{adh}$  and spring constant of the tip-sample interaction  $k_{i,F=0}$  at zero applied load position. We can determine  $k_{i,F=0}$  by calculating the slope  $s$  of the separation force vs distance plot and by using the relation

$$\frac{1}{s} = \frac{1}{k_i} + \frac{1}{k_c} \quad (9)$$

where  $k_c$  is the cantilever spring constant.

The energy dissipated during the separation scan can be calculated by integrating the area encircled by the extend-retract curves<sup>27</sup> in force vs tip-sample separation coordinates.<sup>28</sup> The lower limit of integration is the point where the sample's indentation is zero and the upper limit is the point where the cantilever deflection is the same as on the extend curve.<sup>29</sup> The zero indentation position on the force plot can be obtained noting that

$$\frac{F_{\delta=0}}{F_{adh}} = \frac{8}{9} \quad (10)$$

The friction force was determined from the lateral force traces collected at 10 μm/s, where the tip force on the sample was less than 1 nN.

**IR Spectra Data Collection and Processing.** The IR spectra were collected using a Nicolet 800 series infrared spectrometer continuously purged with nitrogen to remove excess water vapor. IR measurements involved averaging 256 scans with a Happ-Genzel apodization function. Difference spectra were generated by spectral subtraction of copolymer + D<sub>2</sub>O minus D<sub>2</sub>O. Spectral subtraction, to generate difference spectra and to

(25) Aimé, J. P.; Elkaakour, Z.; Odin, C.; Bouhacina, T.; Michel, D.; Curély, J.; Dautant, A. *J. Appl. Phys.* **1994**, *76*, 754–762.

(26) Burnham, N. A. *J. Vac. Sci. Technol., B* **1994**, *12*, 2219.

(27) Marti, A.; Hähner, G.; Spencer, N. D. *Langmuir* **1995**, *11*, 4632.

(28) Ducker, W. A.; Senden, T. J.; Pashley, R. M. *Langmuir* **1992**, *8*, 1831.

(29) Barquins, M.; Maugis D. *J. Adhes.* **1981**, *13*, 53.

(23) Cleveland, J. P.; Manne, S.; Bocek, D.; Hansma, P. K. *Rev. Sci. Instrum.* **1993**, *64*, 403.

(24) Johnson, K. L.; Kendall, K.; Roberts, A. D. *Proc. R. Soc. London, Part A* **1971**, *324*, 301.

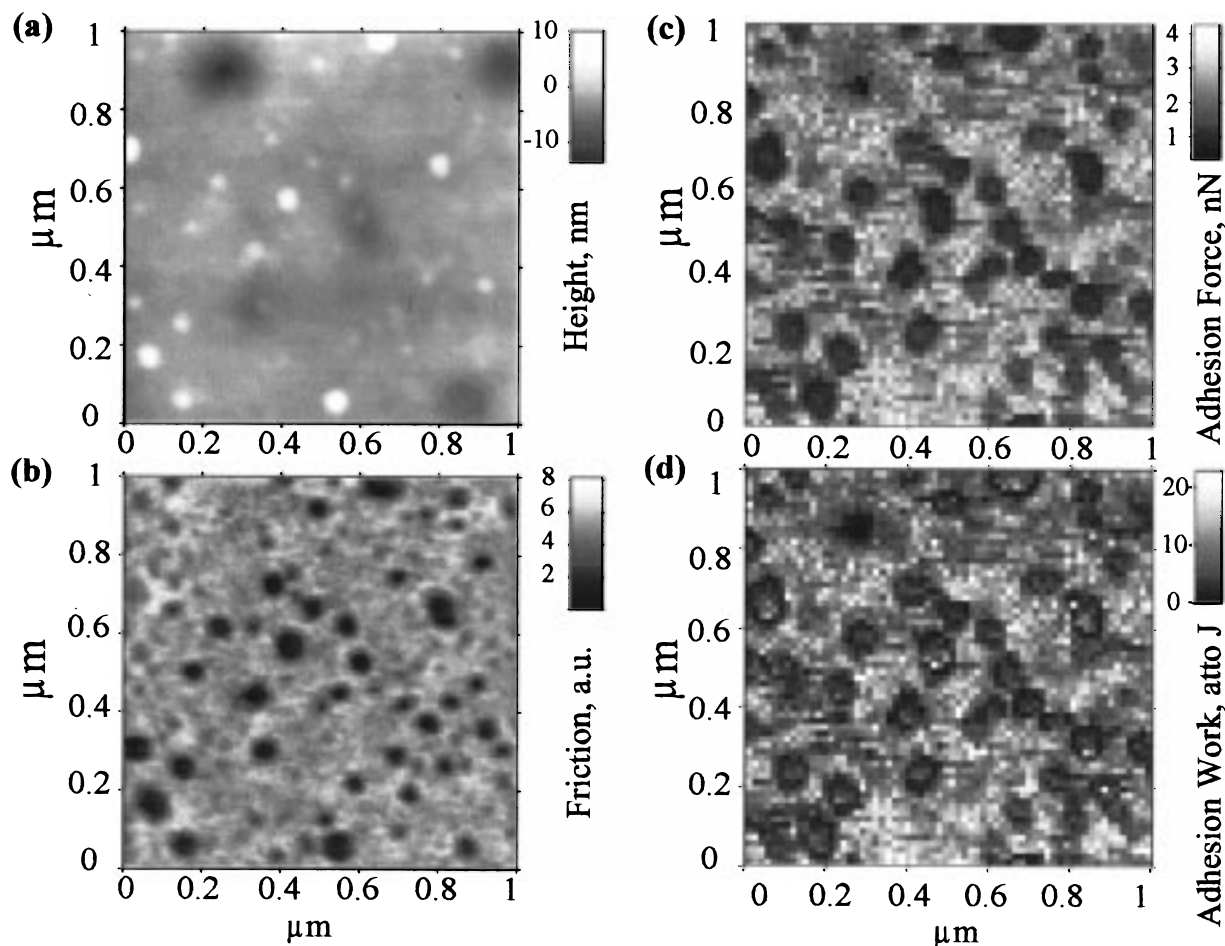


**Figure 1.** Copolymer sample spincast and annealed on mica in 10 mM sodium acetate solution at pH 6.8 using a carboxyl-coated tip: (a) height image obtained using contact mode; (b) friction image of the same area using lateral force microscopy; (c) adhesion force image obtained by analysis of  $64 \times 64$  force vs distance curves collected at the same area as height image, slight offset due to scanner drift, visual and numerical analysis show correlation between these images; (d) energy of adhesion image at the same area as panel c, calculation procedure is described in the text.

remove residual water vapor, was done using Grams/32 software package (Galactic).

### Results and Discussion

**AFM Data. Topography.** Dry films are remarkably smooth, exhibiting only well-separated (ca.  $0.5 \mu\text{m}$ ), small (ca. 20–50 nm deep, 100–400 nm diameter) dimples. The distribution of these dimples is uniform, and annealing above  $T_g$  for 3 days does not remove them.

Films that have been submerged in water develop low, broad particles or pimples that are ca. 10 nm high, and typically 40–100 nm in diameter, separated by 80–200 nm. These particles may be seen as white regions in the height image; see Figure 1a. The particle formation time is at longest several minutes, or within the time required to start imaging after filling the sample cell with aqueous solution. These particles do not disappear when the sample is briefly blown dry under  $\text{N}_2$  or gently rinsed with aqueous solution. Pure polyurethane or fluorinated polyamide films do not show significant change in the surface topography after immersion in water.

**Surface Friction.** The particles show much lower friction than the rest of the surface, seen as dark regions in Figure 1b. The data shown in Figure 1b were acquired using a COOH-coated tip in 10 mM sodium acetate solution; the same effect was observed when we were using uncoated silicon nitride tips in water. These particles, which are regions of partly swollen polymer that can be

moved across the samples when the tip is scanned in hard contact mode, act as a lubricant between the tip and the polymer film below. Phase imaging shows that the particles are much more compliant than the surrounding film. (The Young's modulus of the particles is about a quarter that of the surrounding, flat film as can be concluded from the tapping mode phase detection method.<sup>30,31</sup>)

When polymer surfaces are studied under  $\text{N}_2$  atmosphere the dimples are seen as high friction with the methyl tips and as low friction with the carboxylic acid tips. As one expects, other things being equal, greater friction between two surfaces of similar hydrophobicity,<sup>1–3,32–35</sup> we conclude that the dimples are more hydrophobic. This contrast is not apparent for water-submerged samples.

**Surface Adhesion.** Figure 2 shows examples of the force vs distance plots collected on the wetted polymer surface with carboxyl-coated tip in 10 mM acetic buffer

(30) Overney, R. M.; Leta, D. P.; Pictroski, C. F.; Railovich, M. H.; Liu, Y.; Quinn, J.; Sokolov, J.; Eisenberg, A.; Overney, G. *Phys. Rev. Lett.* **1996**, *76*, 1272.

(31) Maganov, S. N.; Elings, V.; Whangbo, M.-H. *Surf. Sci.* **1997**, *375*.

(32) Friedenberg, M. C.; Mate, C. M. *Langmuir* **1996**, *12*, 6138.

(33) Meager, L.; Pashley, R. M. *Langmuir* **1995**, *11*, 4019.

(34) Yoshizawa, H.; Chen, Y.-L.; Israelachvili, J. *J. Phys. Chem.* **1993**, *97*, 4128.

(35) Yoshizawa, H.; Israelachvili, J. *Thin Solid Films* **1994**, *246*, 71.



**Figure 2.** Typical force plots collected on the polymer surface using a carboxyl-coated tip: (a) Upper panel shows height map with two marks indicating position where force plots were collected, one on the flat area and another on the particle. The lower panel shows two force plots collected at pH 6.8. Differences in adhesion and sample softness between two areas are clearly seen. (b) Approach force plots collected at different pH values are shown. Double layer repulsion can be seen on the force plot curve collected at pH 6.8. There is no noticeable tip-sample repulsion before the contact at pH 4.3.

with pH 6.8. Figure 2a, upper panel, gives the height image. Figure 2a, lower panel, shows one force plot collected on the flat area (solid line), and another force plot on the particle (dashed line). Approach lines are thin; separation lines are thick. These were collected using a "relative trigger", meaning the scanner moves the sample against the tip until a predetermined deflection of the cantilever is achieved with respect to the cantilever deflection at the beginning of the scan. On the "soft" area (particle) the slope of the line after sample is contacted is smaller than on the "hard" (flat area) due to the sample indentation. When the tip contacts the sample, there is rapid indentation of the sample, which can be seen on approach curves. The magnitude of this indentation depends on the sample's elasticity, adhesion energy per unit area, the tip radius, and the cantilever spring constant. For the curves shown, the contact indentation is larger on the particle than on the flat area even though the adhesion force on the particle is smaller. This is an

**Table 1. Adhesion Force (nN) between Several Tip Types and Surfaces**

	bare SiN <sub>x</sub> tip	CH <sub>3</sub> -coated tip	COOH-coated tip
Mica	pure water 0.3	pure water 0.3	~1.1, pH 4 <0.1, pH 7 ~0, pH, 14
copolymer/wet, no buffer	3.1 ± 0.5	18 ± 5	
copolymer/ wet, 10 mM buffer		~20, pH 4.3 ~20, pH 6.8	2.2 ± 0.2, pH 4.3 2.1 ± 0.1, pH 6.8

additional manifestation of the particle's softness relative to the flat area. Approximately 5 nm before the tip contacts the sample, we can see a small rising force (maximum ~0.1 nN). We attribute this force to the electric double layer repulsion.<sup>36,37</sup> Then we fit these repulsion forces with exponential decay function and obtain a characteristic decay length, ~3.3 nm; this length scale corresponds to the Debye length, which is 3 nm<sup>16</sup> for a 10 mM monovalent electrolyte solution. There is no such repulsive force when pH of the buffer is changed to 4.3, i.e., when carboxyl groups on the tip are protonated. Therefore, we conclude that double layer repulsion force is much stronger than probable steric or hydration repulsion forces<sup>16,38</sup> acting on the tip before the tip-sample contact is made. Examples of approach curves near the tip-sample contact at different pH values are shown in Figure 2b. The mean value of the maximum of the repulsive double layer force in 10 mM acetate buffer at pH 6.8 when COO<sup>-</sup>-coated tip approaches the copolymer surface was measured to be 0.13 ± 0.04 nN.

We use the data collected during tip-sample separation motion to extract the adhesion force, the energy of adhesion, and the dissipated energy as described in the AFM data analysis section. For each retract force versus distance plot collected we find the adhesion force  $F_{adh}$  and calculate the slope at the position of zero deflection force by fitting the data with a first-order polynomial. From the fitted line slope and cantilever spring constant we determine the energy of adhesion map, using eqs 9 and 8. This map also can be plotted and analyzed as a histogram. It should be noted that calculation of the spring constant  $k_{i,F=0}$  is accurate only if there is noticeable indentation of the sample. Using eq 10 we find position of zero indentation of the sample and calculate dissipated energy using trapezoidal integration of the data.

Table 1 summarizes the average adhesion force properties of the film surfaces using differently functionalized AFM tips and with different aqueous overlayers. We have found that the adhesion force is greatest when methyl-coated probe tips are used, indicating common hydrophobicity of the surface and tip. Interaction between dipolar tips (carboxylate functionalized) and the surface is much smaller.<sup>39</sup> These data are therefore consistent with the expectation from the contact angle measurements, which indicate a low free energy surface.<sup>14</sup> Figure 1c shows the adhesion force image obtained over the same

(36) Butt, H.-J.; Jaschke, M.; Ducker, W. *Bioelectrochem. Bioenerg.* **1995**, *38*, 191.

(37) Miller, J. D.; Veeramasesaneni; Drelich, J.; Yalamanchili, M. R.; Yamauchi, G. *Polym. Eng. Sci.* **1996**, *36*, 1849.

(38) Marra, J.; Israelachvili, J. *Biochemistry* **1985**, *24*, 4608.

(39) The uncertainties (±1 standard deviation) in measured values of the adhesion force were <0.25 nN for small adhesion forces (<3 nN) between hydrophilic surfaces and increased to as much as ~8 nN for adhesion force greater than 15 nN, such as found between hydrophobic surfaces or when capillary forces are present. Our studies on bare mica reference surfaces show a sigmoidal titration curve indicating that the  $pK_a$  of the tip surface SAM carboxylic acid is ca. 5.

region as shown in parts a and b of Figures 1. The low adhesion force areas correspond to low friction areas in Figure 1b, where a slight offset is due to scanner drifting during collection of force plots. The data collection conditions were otherwise the same. Figure 1d shows the map of the energy of adhesion; the  $7 \pm 1$  atto  $J$  mean value was obtained by averaging six sequential scans, containing 4096 force plots each. The adhesion energy  $W = W_{12}\pi a_{\text{adh}}^2$  map is notably different from the adhesion force map; here, particles appear to have higher adhesion in the center than near the edges. This contrast pattern is not present in the adhesion force map. With the constant adhesion force, adhesion energy depends on  $a_{\text{adh}}$ ,  $W = -a_{\text{adh}}^2 2F_{\text{adh}}/3R$ . From eq 3 it follows that  $a_{\text{adh}}$  is different in the central and the edge areas as a result of the elastic modulus  $K$  difference. The elastic modulus of the sample at the edge of the particles is higher than that in the middle most likely because particles are thinner at the edges.<sup>40</sup>

A comparison of the cantilever deformation work with the dissipated energy during separation ( $25 \pm 2$  atto  $J$  mean) shows that additional energy was dissipated, with higher dissipation at the edges of the particles. The most obvious origin is the sample deformation. Force plots show that the edge effect is mainly due to the copolymer stretching, sometimes accompanied by distance-independent force (see Figure 3). This effect has been seen previously as biomolecules stretching by Gaub and co-workers,<sup>41</sup> and as contamination particle stretching by Hansma and co-workers.<sup>42</sup> We attribute the effect to deformation of the hydrophobic polymer in a poor solvent.<sup>43</sup>

We have also performed pH-dependent studies of the adhesion on copolymer surface, shown in Figure 4. The ionic strength of the aqueous overlayer was kept constant during these measurements. As can be seen from Table 1 the force of adhesion was approximately the same for pH values 4.3 and 6.8. But if the data is analyzed as a histogram, pH dependence can be noted. Figure 4 shows fits of the adhesion force histograms at different pH values with sum of three Gaussian peaks. Mean parameters of the peaks were obtained by averaging the fit parameters of six sequential experiments. The mean position, width, and area fraction of each peak are indicated in the tables in Figure 4. Low values on the histograms correspond to low friction or adhesion areas, which can be seen in Figure 1. The position of each peak does not change with pH, but area does change. The fraction of total adhesion force due to regions of low adhesion force changes with pH as does, necessarily, the fraction due to high adhesion force. When we plot the adhesion force map in only three colors with areas on the map proportional to the histogram peak areas, we can see that low adhesion particles size on the image increases upon pH change from 4.3 to 6.8. This is a consequence of an increase of double layer repulsion near the particle. The carboxylic acid tip undergoes essentially complete ionization state change when exposed to solution pH change from 4.3 to 6.8. The portion of the tip that is just above the tip-sample contact area can experience double layer repulsion from the nearby height feature. This additional repulsion can diminish the adhesion force and increase apparent particle size obtained from the adhesion force mapping. It is known that a carboxylic acid coated tip shows pH-dependent adhesion

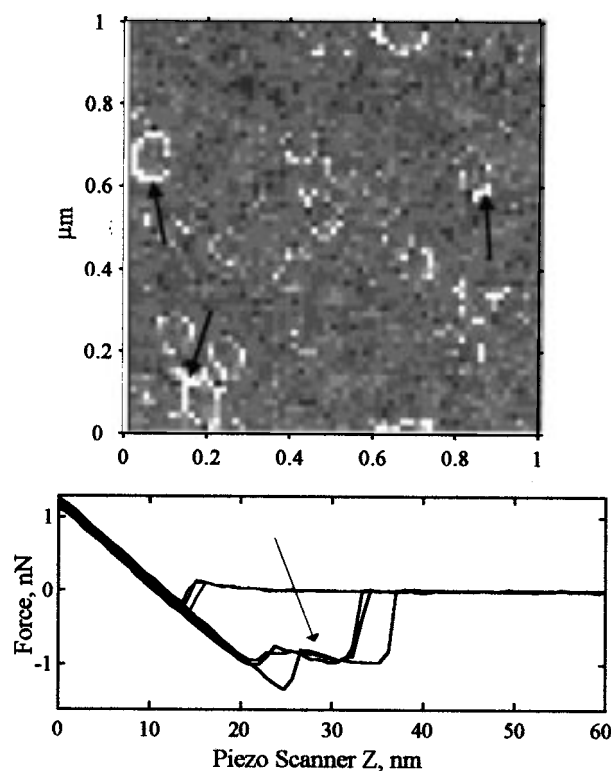


**Figure 3.** Upper panel shows map of the difference between the dissipated energy and the cantilever deformation energy calculated using the same data as used for calculation of adhesion force and adhesion energy maps in Figure 1. Lower panel shows three force plots collected at the sides of the particles. Positions are indicated with arrows on the upper panel. On each of the tip-sample separation force plots there is a part, indicated by arrow, where the deflection force is almost independent of the cantilever position. This means the potential energy of the system is proportional to the tip-sample separation. This type of behavior is a result of exposure of the collapsed polymer in a poor solvent, where the potential energy is proportional to the solvent-sample interfacial area, which is linearly increasing with the tip withdrawing.

on various substrates; double layer repulsion is decreasing the magnitude of the adhesion force.<sup>4</sup> Since we do not see change in the position of the peaks on the histograms, we conclude that the tip reprotonates.

Pressing the tip through the hydrophobic polymer has led to a local  $pK_a$  change for the SAM carboxylic acids. By way of analogy, we note that the  $pK_a$  of acetic acid shifts by 4  $pK_a$  units when dissolved in solutions of between 0 and 70% dioxane in water.<sup>44</sup> It is possible that at solution pH 6.8, the tip may partly protonate as it contacts the polymer, due to the lower water concentration between the tip and the polymer compared with the aqueous overlayer. This reprotonation could explain why the adhesion force Gaussian bands do not shift while the tip changes its ionic state. The polymers themselves do not have functional groups that can be ionized over this pH range.

**IR Spectroscopy of Hydrating Films.** Figure 5 shows a representative infrared spectrum of a 1–2  $\mu\text{m}$  thick spin cast and annealed film of the poly (amide-urethane) copolymer in Chart 1. The vibrational band assignments are conventional.<sup>45</sup> Figure 5 also shows how

(40) Akhremitchev, B. B.; Walker, G. C. Effect of finite sample thickness on elasticity determination using atomic force microscopy. Submitted for publication in *Langmuir*.

(41) Rief, M.; Gautel, M.; Oesterhelt, F.; Fernandez, J. M.; Gaub, H. E. *Science* **1997**, *276*, 1109.

(42) Radmacher, M.; Cleveland, J. P.; Fritz, M.; Hansma, H. G.; Hansma, P. K. *Biophys. J.* **1994**, *66*, 2159.

(43) Halperin, A.; Zhulina, E. B. *Europhys. Lett.* **1991**, *15*, 417.

(44) Creighton, T. E. *Proteins*; Freeman and Co., New York, 1993; p 144.

(45) Urban, M. W. *Vibrational Spectroscopy of Molecules and Macromolecules on Surfaces*; Wiley: New York, 1993 and references therein.

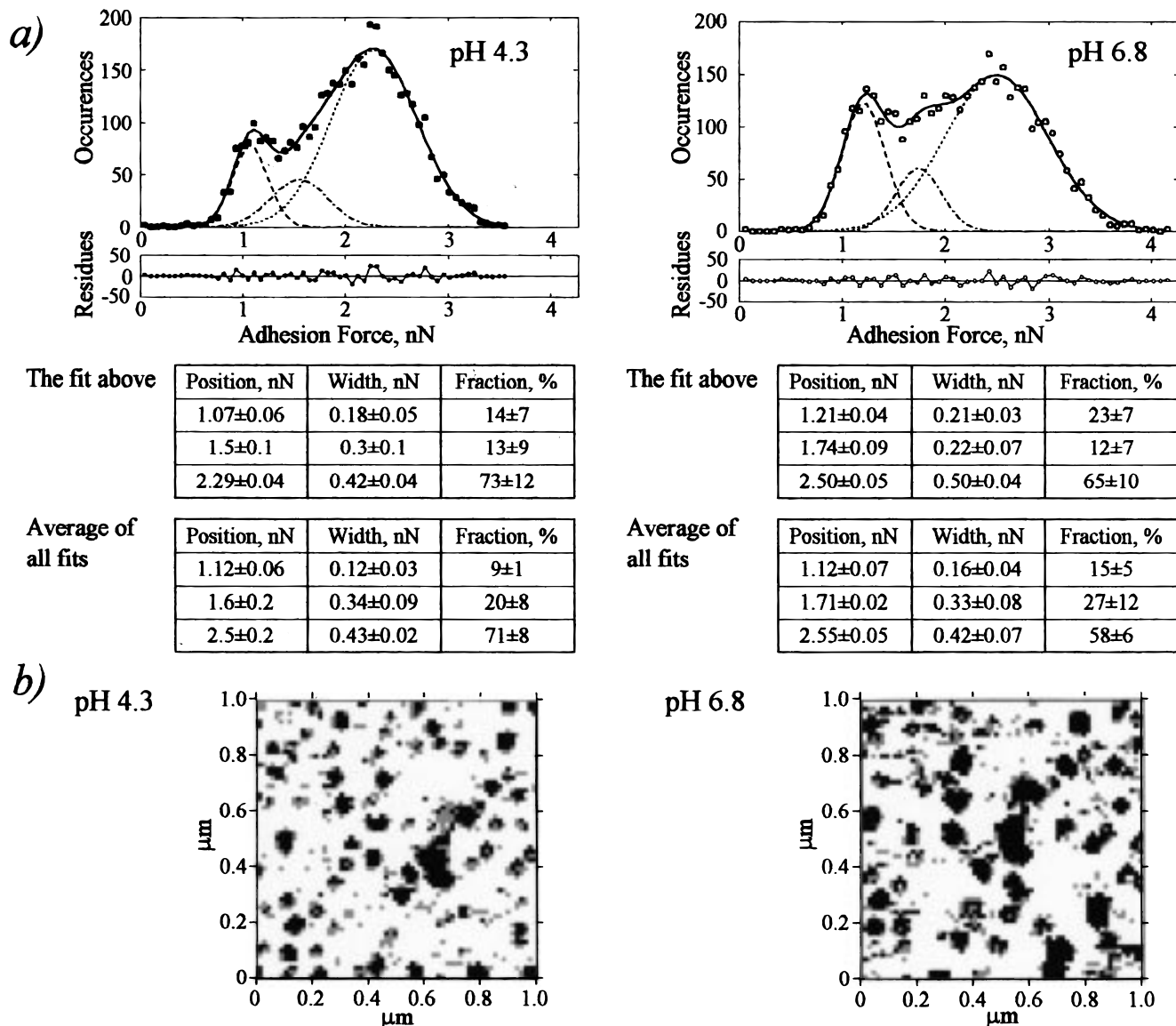


**Figure 4.** (a) Typical histograms of the force of adhesion calculated from analysis of force plots which were obtained on the copolymer surface with a carboxyl-coated tip in 10 mM acetic buffer. pH is indicated. The histograms may be approximately fit by the sum of three Gaussians. The residual error to these fits is shown below each histogram. The figure includes tables with the fit parameters: the position, width, and fraction of the area under the peak are given for each Gaussian band. Upper tables include parameters for the displayed histogram, where error is estimated as  $\sigma$ , standard deviation, obtained from the fit error matrix. Lower tables show mean parameters in a six-member series of experiments conducted on the different areas of the sample. Errors here were estimated as the standard deviation from the mean value in the series. (b) Three-shade map of the adhesion force collected at different pH values. Area occupied by each shade is proportional to the area under each Gaussian band obtained from the fitting. Dark shades correspond to low adhesion force values. This shows that apparent particle size is increasing as a result of the double layer repulsion at pH 6.8 compared with the map collected at pH 4.3.

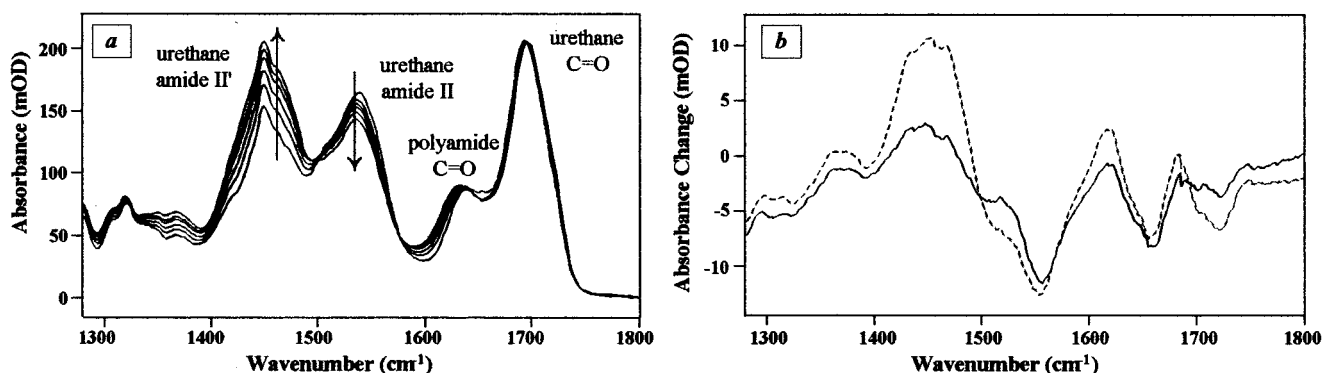
the copolymer IR spectra are affected by exposure to  $D_2O$ , monitored by urethane H/D exchange. The greater IR absorbance is seen at urethane carbonyl resonances because that block is exchanging H for D at the amide nitrogen. Decrease of urethane CO/NH combination band absorption and increase of urethane CO/ND combination band absorption are also clearly visible at 1550 and 1450  $cm^{-1}$ , respectively. The difference between the IR spectra taken at 3 and 6 min following film immersion exhibit changes in the polyamide block carbonyl absorption region at 1650  $cm^{-1}$ ; see Figure 5b. Thus,  $D_2O$  is perturbing both blocks. The IR changes involve ca. 7% of the sample carbonyl chromophores, which exceeds the percentage of sample carbonyl chromophores found in the particles.

Figure 5b also shows the long time difference spectrum (1 h minus 6 min). This difference spectrum illustrates

the consequences of extended water penetration and copolymer relaxation. This difference spectrum shares the principal features of the difference spectrum mentioned above. Thus both short and long time dynamics involve both blocks.

The polymer response to immersion occurs on a range of time scales. In general, there are hydration dynamics on a less than 3 min time scale, 30 min time scale, several hour time scale, and many day time scale (see Supporting Information). The time scales for these surface and IR changes correlate with the time scales for contact angle hysteresis observed by Chapman and Marra.<sup>14</sup>

**Origin of the Early Contact Angle Hysteresis.** We now address whether the particle formation can account for the contact angle hysteresis. In what follows we assume that after immersion the surface is composed of



**Figure 5.** (a) Time-dependent IR spectra of a copolymer film following continuous immersion in  $D_2O$ . Shown are traces collected 3 min, 1 h, 2 h, 4 h, 6 h, and 11 h after immersion. The  $D_2O$  background from the  $6 \mu m$  path length cell has been subtracted to reveal the changes in the copolymer functional group absorbances. The principal features are changes of the amide CO absorbance at ca.  $1636\text{--}1660 \text{ cm}^{-1}$ , the urethane CO/NH combination band at  $1550 \text{ cm}^{-1}$ ; and CO/ND combination band at  $1450 \text{ cm}^{-1}$ . The last two are evidence of H/D isotopic exchange. (b) IR difference spectra: solid line, 6 min minus 3 min (scaled  $3\times$ ) showing changes due to surface particles; dashed line, 1 h minus 6 min, showing changes due to underlying film. Both early time and late time hydration affect both copolymer blocks.

two principal types areas, with relative areas 29:71 corresponding to areas with and without particles. According to Adamson,<sup>46</sup> for a composite surface,

$$\cos(\theta_{\text{exp}}) = r \cos(\theta_{\text{true}}) = f_1 \cos(\theta_1) + f_2 \cos(\theta_2) \quad (11)$$

where  $f_1$  and  $f_2$  correspond to the fractional area of each type,  $r$  is an empirical roughness parameter, and  $\theta$  is the contact angle. The relevant experimental contact angle for this surface,  $\theta_{\text{exp}}$ , is the receding contact angle,  $48.6^\circ$ .<sup>14</sup> Following eq 11, the contact angle on the nonparticle area, which covers 71% of the surface, must be less than  $57^\circ$ . This analysis suggests that it is unlikely that particle formation can account for the majority of the contact angle hysteresis,  $60^\circ$ . Instead there must be significant surface polarization change in nonparticle areas.

Several groups<sup>17,37,47,48</sup> have recently considered the effect on contact angle hysteresis of nanoscale roughness. Webber and co-workers, who examined micelles adsorbed onto polystyrene surfaces, found that  $r$ , as seen in eq 11, can be as large as 1.88 for dense coverage by ca. 50 nm diameter micelles. At our particle coverage, ca. 30%,  $r$  would be 1.2, making a linear interpolation. Thus we conclude that both roughness and surface polarization in nonparticle areas contribute to early contact angle hysteresis on poly(amide urethane) film surfaces.

(46) Adamson, A. W. *Physical Chemistry of Surfaces*; Wiley: New York, 1982.

(47) Andrade, J. D. *J. Int. Mater. Sys. Str.* **1994**, *5*, 612.

(48) Tang, J. Z.; Harris, J. G. *J. Chem. Phys.* **1995**, *103*, 8201.

### Summary and Conclusions

The hydration dynamics of low-energy surfaces have been characterized by atomic force microscopy and infrared spectroscopy of submerged films. Shallow surface dimples exhibit low friction to carboxylate or carboxylic acid functionalized probe tips under  $N_2$ . Compliant, ca. 10 nm high particles of swollen copolymer with a dispersion of characteristic lateral radii are formed within minutes of film submersion in aqueous solutions. These particle features do not grow significantly on longer time scales, up to days. Underwater copolymer film surfaces exhibit distinct regions of low and high force of adhesion. We used a Gaussian model to fit the force of adhesion probability distribution. The relative area dependence under bands of low and high adhesion force on ionic state of the chemically modified tip is related to the apparent particle size in the adhesion force map. The pH-independent position of the most probable adhesion forces is explained by a  $pK_a$  shift of the carboxylate-coated tip during the tip-sample contact. Infrared spectroscopy of these films reveals that both copolymer blocks are perturbed by hydration. The particles and water-induced polarization of flat regions of the surface are both responsible for the early decrease in contact angle.

**Supporting Information Available:** Table providing details of the experimental fits to the infrared absorption data (1 page). Ordering information is given on any current masthead page.

LA970911V